Physical modeling of anisotropic domains: Ultrasonic imaging of laser-etched fractures in glass

Robert R. Stewart (University of Houston), Nikolay Dyaur (University of Houston), Bode Omoboya (University of Houston), J. J. S. de Figueiredo (Unicamp-Brazil and University of Houston), Mark Willis (ConocoPhillips, Houston), and Samik Sil (ConocoPhillips, Houston)*

Summary

Physical modeling, using ultrasonic sources and receivers over scaled exploration structures, plays a useful role in wave propagation and elastic property investigations. This paper explores the anisotropic response of novel fractured glass blocks created with a laser-etching technique. We compare transmitted and reflected signals for P- and S-waves from fractured and unfractured zones in a suite of ultrasonic experiments. The unaltered glass velocities are 5801 m/s and 3448 m/s for P and S waves, respectively, with fractured zones showing a small decrease (about 1%). Signals propagating through the fractured zone have decreased amplitudes and increased coda signatures. Reflection surveys (zero-offset and variable polarization and offset gathers) record significant scatter from the fractured zones. The glass specimens with laser-etched fractures display a rich anisotropic response.

Introduction

Heterogeneous layering in the earth or discrete fractured zones can exhibit significant complexity in properties and seismic response. To better understand these zones and their structure, physical modeling has been used as a useful tool. Recent numerical and physical modeling studies (Willis et al., 2006; Burns et al., 2007) have shown that scattered energy, induced by short wavelength features, can assist in delineating fracture zones. Wong et al. (2009) used phenolic laminate to simulate thinly layered regions in physical modeling studies, while Tatham et al. (1992) and Ebrom et al. (1990) employed stacked Plexiglas plates to model an effective anisotropic fractured medium. Rathore et al. (1994) prepared an anisotropic synthetic sandstone with known crack geometry and dimension. In our case, we begin with homogeneous glass blocks, then using laser-etching techniques, create domains or regions of fractures with various densities, orientation, and structures. The placement of the "cracks" or "fractures" created by the laser-etching process can be controlled very precisely. However, some experience is required to not break the glass entirely in the etching process (the laser-etching procedure actually melts many, very small dots of glass to create the fault planes). The first part of the work reported here determines the velocity, from transmitted energy, of the various anisotropic blocks. Next, we record transmissions in a 3D-type geometry to produce time slices on and off the fractured regions. We then move to reflection geometries, for P and S-waves, including various 2D and 3D surveys over the anomalous areas in the fractured blocks.

Experimental method and models

The experiments were carried out using the ultrasonic physical modeling facilities at the Allied Geophysical Laboratories at the University of Houston. We first employed an ultrasonic pulse transmission technique for determination of compressional- and shear-wave velocities. The ultrasonic system includes a pulser/receiver 5077PR, digital oscilloscope HS-4 (50 MHz), low-noise preamplifiers and transducers of P and S-wave with central frequencies of 1 MHz. A similar experimental setup uses ultrasonic pulse-echo and offset measurements with a variety of transducers (100 kHz, 1.0 MHz, and 5.0 MHz). A scaling factor of 1:10000 for time and space upscaling or for frequency downscaling is often used to make the measurements more accessible to standard seismic values. We have built ten different laser-etched models (e.g., Figures 1 and 2). The intention of the laser etching is to produce discrete anisotropic and scattering domains.

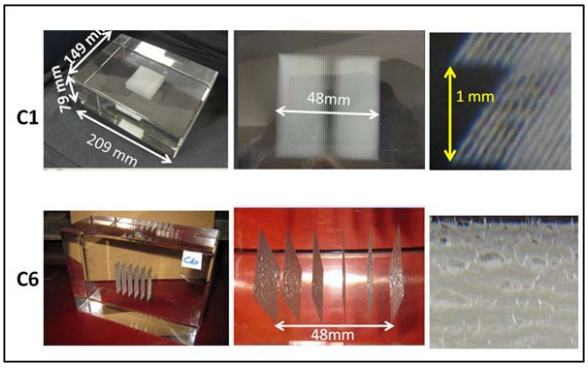

Figure 1. Glass models with laser-etched, internal fractures or cracks at different densities (spacings). Model C1 has 48 fracture planes and model C6 has 6 fracture planes.

Figure 2. Two further glass models with laser-etched interior fracture zones simulating VTI and HTI regions.

The size of the glass blocks is 209 x 149 x 79 mm and the overall dimension of the fracture zones in models C1 and C6 was 48 x 48 x 26 mm (with a spacing of 1 mm between fractures in C1 while model C6 has spacings of 10 mm). The fractured areas are kept in the center of the blocks to allow the measurements to be recorded with a minimum of interference from reflections from the block edges. We use variable spacings (and transducer frequencies) to investigate relatively long and short ultrasonic wavelengths as compared to the fracture spacing. Other fractured blocks have more complicated levels, domains, and orientations of fractures. The fractured areas are intended to simulate domains of VTI, HTI, and higher-order symmetries.

Ultrasonic measurements

Our first measurements use direct transmission of energy across various faces of the block. Figure 3 shows the P-and S-wave velocities for the glass model C1 in three orthogonal directions X, Y, and Z. For each direction, three measurements were made with P and S source and receiver transducers oriented parallel to each other. The velocity for the blank (or unfractured) glass zones (with paths named X, Y, Z) had average values of Vp = 5801 m/s and Vs = 3448 m/s. The waves travelling through the fracture zones (with paths Xf and Yf) were slightly slower and had decreasing arrival amplitudes.

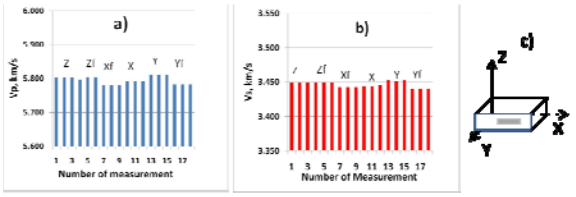

Figure 3. Model C1 a) P-wave velocity and b) S-wave velocity in blank glass (X, Y, and Z) and in directions through the fractured zone (Xf, Yf, and Zf), c) orientation of the glass model. Note that these are average velocities through the full blocks.

Comparing the velocities through the blank glass versus fracture zone for model C1, we found decreases in the P-wave velocity of up to 1.2% within the fracture zone. The largest decrease of P-velocity was in direction X, normal to fracture layers. From time picking and length measurement error, we estimate that the error in the calculated group velocities (V_P and V_S) was less than 0.4%. This also coincides with the variation among repeated measurements. We observed a decrease in the P-velocity of 0.7% (compared to the unfractured glass) parallel to fracture layers in the Y direction. We also measured variation in the S-wave velocity (V_{S1} = 3438 m/s parallel to fractures and V_{S2} = 3418 m/s for polarization normal to fractures). No such variation was evident in the unfractured blank glass. While these velocity variations are small, they are consistent across many experiments.

Transmission Imaging

Several 3D transmission surveys were on conducted on two glass models (models C4 and C3). The transmission experiment was in a "marine" setting (in a water-filled tank) with 300 kHz spherical transducers as both source and receiver. The transducers were placed on opposite sides of the glass blocks and we used the blank glass for calibration and comparison (Figure 4).

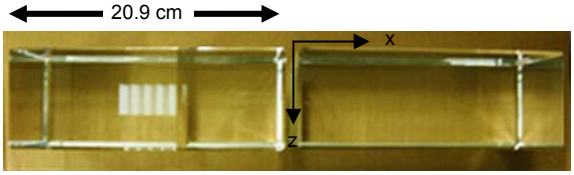

Figure 4: Glass models C4 (with a small fracture set and large crack) and C3 (the unfractured comparison block).

A schematic diagram of the 2D transmission geometry is displayed in Figure 5. The two blocks were separated by 10 cm and submersed in water.

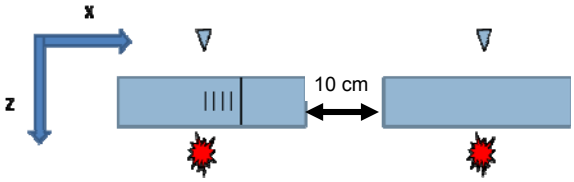

Figure 5: Schematic diagram of the transmission survey on glass models C4 and C3 side-by-side with 10cm separation. Source and receivers are on opposing sides of the blocks.

Figure 6 shows a resulting transmission section of the two side-by-side blocks. We note the diffraction from the large crack and fracture set on the left section. The blocks have slightly different thicknesses and internal velocities.

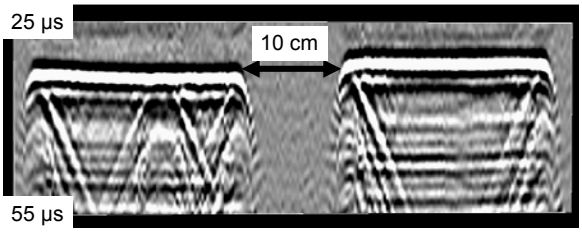

Figure 6. Transmission section of models C4 (left) and C3 (right). Notice the diffraction, on C4, due to a large vertical crack.

Assembling a number of 2D, zero-offset transmission sections produces a 3D data volume (i.e., the surveys were conducted over the full 2D area of the blocks). We then

search through the transmission data volume to find the onset of fracture-related events. Figure 7 shows the amplitudes transmitted through the calibrating block on the right (very little energy loss). On the left, we see regions of attenuated signal (black) which we attribute to the effects of fracturing.

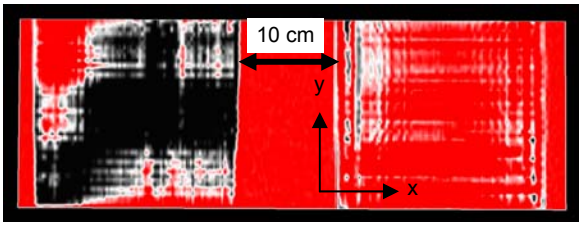

Figure 7. Time slice display at 32 µs (plan view) of models C4 (left) and C3 (right). Notice the altered amplitudes in black on the left due to the one large crack and embedded fractures.

Zero-offset reflection experiments

We next move on to assessing reflected energy. In studying the response of the fractured zones, we found that at frequency 1.0 MHz there were strong reflections and scatter for P- and S-waves (Figure 8 and 9) from the fractured regions. In model C6, we see that the amplitude of the reflected signal increases as we approach the fractured zone and the amplitude of bottom reflected signal decreases. There may be scattering attenuation when the wave propagation is normal to the fracture plane (Mavko et al., 1998). We also observed similar behavior for the S-wave. S-wave reflections from fractures were better defined than P-wave reflections for model C6.

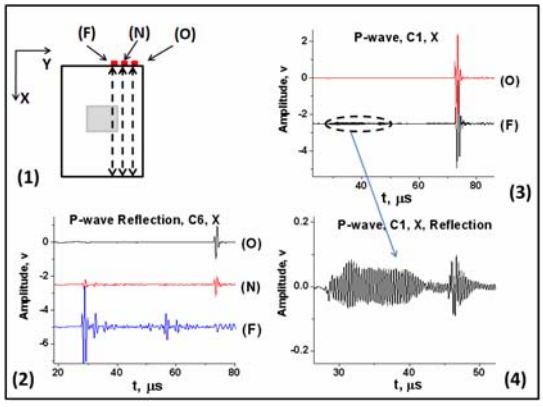

Figure 8. Waveforms of the 1 MHz P-wave in the X direction: (1) Schematic of the measurements – (O) off fracture, (N) near fracture, and (F) on fracture zone; (2) Model C6 waveforms in (O), (N), and (F) positions; (3) Model C1 waveforms in (O) and (F) positions; (4) Zoom view of Model C1 reflections from the fracture zone in the (F) position.

Interestingly, the central frequency of the source for both P- and S-waves was 1.0 MHz, but the spectrum of the dominant reflected signal from the fracture zone seems to be weighted toward higher frequencies for model C1.

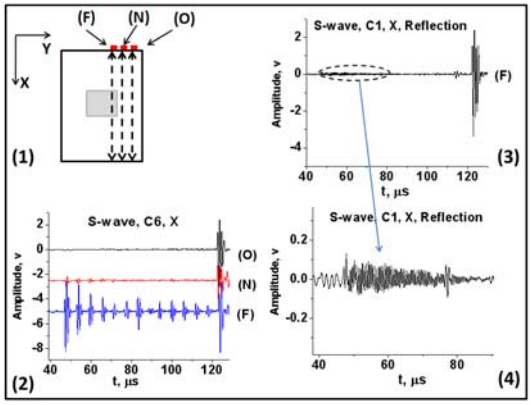

Figure 9. Waveforms of the 1 MHz S-wave in the X direction: (1) Schematic of the measurements – (O) off fracture, (N) near fracture, and (F) on fracture zone; (2) Model C6 waveforms in (O), (N), and (F) positions; (3) Model C1 waveform in the (F) position; (4) Zoom view of Model C1 reflections from the fracture zone in the (F) position.

Depending on the structure of the fracture zone and especially on the spacing of fracture layers, we have recorded different responses for P- and S-waves. When the ratio of wavelength to fracture spacing varies, there are correspondent changes in amplitude.

Further pulse-echo (zero-offset) measurements were performed in the X and Y directions using 5 MHz and 1 MHz P-wave transducers. In the X direction, the P-wave propagates perpendicular to the direction of fracture planes versus parallel in the Y direction. Figure 10 shows the P-wave section obtained for the models C1 and C6 in the Y direction. In model C1, the top and bottom of the fracture region can be interpreted clearly. For model C6, only the top of fracture boundary was imaged. The ultrasonic wavelength (1.2 mm) is much less than the fracture separation (10 mm) and hence each fracture edge appears to act as a scatter point. Multiple reflections inside the fracture sets make it complicated to interpret the bottom of the fracture zone. The coda wave is also very prominent below the fracture zone arrivals.

The section in Figure 11 indicates that the P-wave energy in Models C1 and C6 in the X direction is attenuated in the fractured region. For model C6, part of energy is reflected and scattered in the first fracture and multiple reflections are observed with other fractures. Two features become apparent: With fracture density at about two fractures per

wavelength, tuning effects start to arise as well as amplitude decreases. Furthermore, the coda wave is reduced when the fracture plane is perpendicular to the wave propagation direction. Thus, the coda wave may assist us in fracture location and description.

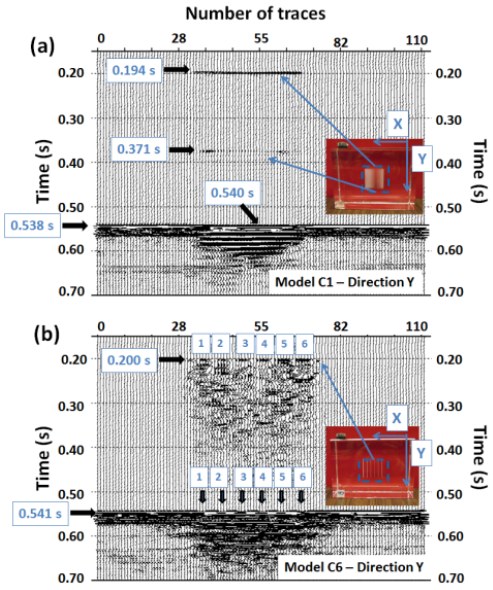

Figure 10. Zero-offset P-wave reflection sections using a 5 MHz transducer. (a) Model C1 and (b) Model C6. In both cases, the propagation direction is parallel to the fracture plane.

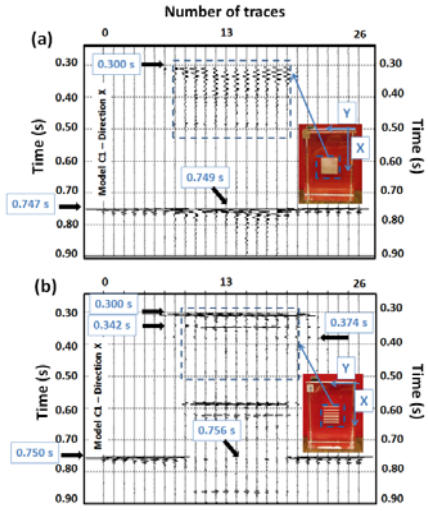

Figure 11. Zero-offset P-wave seismograms using a 5 MHz transducer. (a) Model C1 and (b) Model C6. In both cases, the propagation direction is perpendicular to the fracture plane.

Sections in Figure 12 indicate that the top and bottom of the C1 fracture zone can be imaged. However, even though fracture boundaries for C6 cannot be resolved, the strong coda wave may detect them.

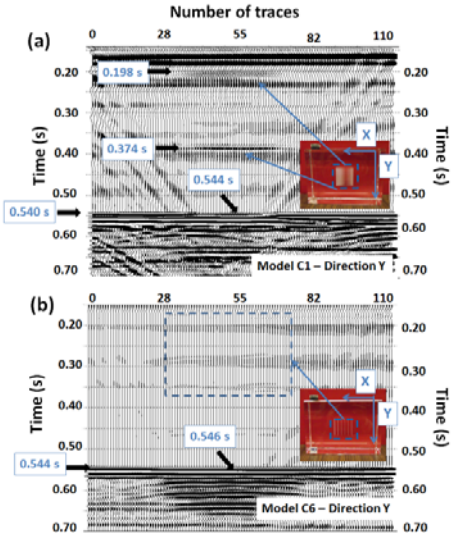

Figure 12. P-wave seismograms using a 1 MHz transducer. (a) Model C1 and (b) Model C6. In both cases, the P-wave propagation was parallel to the fractures.

Conclusions

We have developed novel laser-etched glass models to simulate fracture domains. Ultrasonic surveying of these physical models displays a number of fascinating phenomena related to the transmission, reflection, and scattering of waves from the anisotropic cracked or fractured zones. Fracturing causes a small decrease in the transmitted velocities, but significant development of scattered or reflected energy. There are hints of frequency dependence on fracture density. The coda signature may also be an indicator of the fracture orientation and density. The flexibility of creating complicated anisotropic models with this new laser-etching technique and then ultrasonic modeling over them is a very exciting procedure for fracture and anisotropy studies.

Acknowledgments

This research was generously supported by ConocoPhillips and the Allied Geophysical Laboratories (AGL) and its sponsors at the University of Houston. We are grateful to the AGL staff, Anoop William and Robert Wiley, for their assistance with the experiments. We thank Kasper van Wijk for foundational discussions on the laser etching of fractures in physical modeling.

EDITED REFERENCES

Note: This reference list is a copy-edited version of the reference list submitted by the author. Reference lists for the 2011 SEG Technical Program Expanded Abstracts have been copy edited so that references provided with the online metadata for each paper will achieve a high degree of linking to cited sources that appear on the Web.

REFERENCES

Burns, D. R., M. E. Willis, M. N. Toksoz, L. Vetri, and S. Donato, 2007, Fracture properties from seismic scattering: The Leading Edge, **26**, 1186–1196, doi:10.1190/1.2780790.

Ebrom, D. A., R. H. Tatham, K. K. Sekharan, J. A. McDonald, and G. H. F. Gardner, 1990, Hyperbolic traveltime analysis of first arrivals in an azimuthally anisotropic medium: A physical modeling study: Geophysics, **55**, 185–191, doi:10.1190/1.1442825.

Mavko, G., T. Mukerji, and J. Dvorkin, 1998, The rock physics handbook: Tools for seismic analysis in porous media: University of Cambridge.

Rathore, J. S., E. Fjaer, R. M. Holt, and L. Renlie, 1995, P- and S-wave anisotropy of synthetic sandstone with controlled crack geometry: Geophysical Prospecting, **43**, no. 6, 711–728, doi:10.1111/j.1365-2478.1995.tb00276.x.

Willis, M. E., D. R. Burns, R. Rao, B. Minsley, M. N. Toksöz, and L. Vetri, 2006, Spatial orientation and distribution of reservoir fractures from scattered seismic energy: Geophysics, **71**, no. 5, O43–O51, doi:10.1190/1.2235977.

Wong, J., K. W. Hall, E. V. Gallant, R. Maier, M. B. Bertram, and D. C. Lawton, 2009, Seismic physical modeling at the University of Calgary: CSEG Recorder, **3**, 36–43.